Research Square

Preprints are preliminary reports that have not undergone peer review.
They should not be considered conclusive, used to inform clinical practice,
or referenced by the media as validated information.

Conditional Phase Sensitivity and Atom–RestCorrelations in a Diamond Four-LevelOptomechanical Cavity

Syed Jamal Anwar

sjamalanwar@gmail.com

Quaid-i-Azam University

S. Abdul Khalek S. Abdul Khalek

Taif University

Research Article

Keywords:

Posted Date: November 6th, 2026

DOI: https://doi.org/10.21203/rs.3.rs-11404553/v1

License: This work is licensed under a Creative Commons Attribution 4.0 International License.
Read Full License

Additional Declarations: No competing interests reported.

Conditional Phase Sensitivity and Atom–Rest Correlations in a Diamond Four-Level Optomechanical Cavity

S. Jamal Anwar[1] and S. Abdul Khalek[2]

[1]Department of Physics, Quaid-i-Azam University, Islamabad 45320, Pakistan

[2]Department of Mathematics and Statistics, College of Science, Taif University, P.O. Box 11099, Taif 21944, Saudi Arabia

Corresponding author: S. Jamal Anwar; sjamalanwar@gmail.com

October 7, 2026

Abstract

We investigate how phase information initially stored in a diamond four-level atom is redistributed when the atom interacts with a quantized cavity field and a mechanical mode. The phase ϕ is encoded in the atomic superposition $(|1\rangle + e^{i\phi}|2\rangle)/\sqrt{2}$, while the optical and mechanical subsystems start in Fock states. The dynamics are generated by a coarse-grained optomechanical Hamiltonian together with normalized non-Hermitian no-jump evolution. A central point of the analysis is that the induced $|2\rangle \leftrightarrow |3\rangle$ channel contains the distinct photon operators $a^{\dagger k}a^k$ and $a^k a^{\dagger k}$; they cannot be merged without changing the dynamics. The numerical study is deliberately restricted to the stationary, single-photon case $k = 1$, for which the calculation is reproducible and the Hilbert-space truncation can be checked directly. We track the reduced-atomic quantum Fisher information (QFI), von Neumann entropy, purity, and total l_1 coherence. In the parameter range considered, increasing the optomechanical coupling G reduces the maximum conditioned atom–rest entropy from about 1.676 to 0.374 bits and raises the minimum atomic purity from about 0.356 to 0.876. At the same time, the time-averaged local QFI decreases from about 0.450 to 0.336, while the mean total coherence changes only weakly and non-monotonically. Thus stronger optomechanical coupling does not improve all quantum resources simultaneously: it keeps the conditioned atomic state purer and less entangled with the rest, but it also reduces the amount of phase information locally accessible from the atom. To expose this contrast more clearly, the time-dependent observables are plotted for two complementary combinations of G values, and the full nine-point coupling scan is summarized separately.

Keywords: quantum Fisher information; diamond four-level atom; cavity optomechanics; conditional dynamics; entanglement entropy; quantum coherence

1 Introduction

The interaction between a discrete quantum emitter and a quantized electromagnetic mode is one of the basic settings in quantum optics. In its simplest form, the Jaynes–Cummings model explains coherent atom–field exchange, vacuum Rabi oscillations, and the well-known collapse-and-revival structure of a quantized field interacting with an atom [1, 2, 4, 5, 6]. The same model also provides a useful starting point for understanding how information moves between matter and light. Once additional atomic levels, nonclassical fields, nonlinear interactions, or multiphoton transitions are included, that exchange becomes considerably richer and the reduced state of the atom can carry signatures that are not visible from populations alone [7, 8, 9, 12, 19, 64].

Multilevel atoms are especially interesting because the same initial excitation can follow more than one coherent pathway. A diamond four-level atom contains an upper state $|1\rangle$, two intermediate states $|2\rangle$ and $|3\rangle$, and a lower state $|4\rangle$. The upper state is coupled to both intermediate states, and both intermediate states are coupled to the lower state. This geometry allows amplitudes to interfere and makes coherence transfer more structured than in a two-level system. Diamond-type configurations have therefore appeared in studies of coherent control, cavity QED, electromagnetically induced transparency, and nonlinear photon interactions [17, 18, 20, 21, 22]. They are also relevant to quantum interfaces, where one wants to understand not only whether an excitation is transferred, but how much phase information remains in a chosen subsystem after the transfer [23].

A second ingredient in the present problem is optomechanics. In cavity optomechanics, the photon number couples to mechanical displacement through radiation pressure. This interaction can cool a mechanical oscillator, modify the optical spectrum, generate nonlinear behavior, and mediate correlations between optical, atomic, and mechanical degrees of freedom [34, 35, 36, 37]. The Hamiltonian origin of the radiation-pressure term can be derived from a movable cavity boundary [65], and early work already showed that a movable mirror can support nonclassical states and become entangled with a cavity field [66, 67, 68]. Hybrid atom–mechanical proposals extend this idea by using the cavity field as the channel through which microscopic atomic variables communicate with a mesoscopic mechanical oscillator [38, 39, 42, 43]. This is precisely the regime in which it becomes useful to ask which quantum properties are shared, which remain local, and which are suppressed as the coupling is changed.

Entanglement is one natural way of describing such redistribution. Its conceptual roots lie in the Einstein–Podolsky–Rosen argument and Bell's theorem [24, 25], while modern quantum-information theory provides several quantitative measures and operational interpretations [26, 27, 50, 51, 32, 33]. For a globally pure bipartite state, the von Neumann entropy of either reduced subsystem is a direct entanglement measure. This fact is particularly useful in a conditioned no-jump trajectory: after normalization, the global conditional state remains pure, so the reduced atomic entropy measures atom-versus-rest entanglement rather than classical mixing caused by an ensemble average. This distinction matters because a non-Hermitian no-jump calculation is not the same object as a Lindblad master-equation solution. Quantum-trajectory theory makes clear that the two descriptions answer different physical questions

[30, 31, 61, 62, 63].

For parameter estimation, quantum Fisher information provides a complementary view. QFI quantifies the sensitivity of a quantum state to a parameter and sets the quantum Cramer–Rao bound for the best possible precision [44, 45, 56, 57]. In quantum metrology, a large QFI means that nearby parameter values produce states that are easier to distinguish. This idea has been used extensively in quantum-enhanced sensing and in studies connecting metrological usefulness with entanglement and other many-body resources [46, 47, 48, 49, 52, 53, 58]. In the present system the estimated quantity is not a mechanical damping rate or a coupling constant. It is the relative phase ϕ written into the initial atomic superposition. We therefore ask a direct question: after the atom has interacted with the cavity and mechanical modes, how much of that original phase information can still be accessed from the atom alone?

Coherence adds a third, related but distinct, viewpoint. In a four-level system it is risky to follow only one off-diagonal density-matrix element. Interaction can transfer coherence from one pair of levels to another, so a decrease of $|\rho_{12}|$ does not necessarily mean that the atom has lost its total coherent content. We therefore use the l_1 norm of coherence, which sums the magnitudes of all off-diagonal elements in the chosen atomic basis [59, 60]. Together, QFI, entropy, purity, and total coherence tell a more balanced story than any one of them can provide by itself.

Recent work has brought QFI and multiphoton interactions into hybrid optomechanical models [54] and has considered the QFI of a diamond-type four-level atom in an optomechanical cavity [55]. That line of work motivates a careful look at the effective Hamiltonian used for the intermediate-state dynamics. The point is technical but physically important. The induced $|2\rangle \leftrightarrow |3\rangle$ coupling contains two photon-number operators, $a^{\dagger k}a^k$ and $a^k a^{\dagger k}$. They are different operators. For $k = 1$, $aa^\dagger = a^\dagger a + 1$. If these factors are incorrectly treated as identical, a finite interaction can disappear when equal atom–field couplings are assumed. Because that channel contributes to amplitude and coherence transfer, the ordering of the operators must be retained before numerical trends are interpreted.

The aim of this paper is therefore modest but precise. We analyze a stationary diamond four-level atom coupled to one cavity mode and one mechanical mode using the corrected coarse-grained Hamiltonian and normalized no-jump dynamics. The formal Hamiltonian is written for k-photon processes, but every numerical figure presented here uses $k = 1$. We vary the optomechanical coefficient G and examine how local phase sensitivity, conditioned atom–rest entanglement, purity, and total atomic coherence change. The main result is not a universal enhancement with increasing G. Instead, stronger coupling makes the conditioned atomic subsystem appreciably purer and less entangled with the rest, while its time-averaged local QFI falls moderately and its total coherence remains comparatively stable. The expanded physical discussion below emphasizes why these statements are compatible rather than contradictory.

2 Physical model and effective Hamiltonian

We consider a diamond four-level atom interacting with a single quantized cavity mode and a single mechanical mode. The construction combines standard cavity-QED light–matter coupling, the diamond-level topology, multiphoton Jaynes–Cummings-type interactions, and radiation-pressure optomechanics [1, 3, 18, 34, 35, 65, 54, 55]. With $\hbar = 1$, a microscopic starting Hamiltonian is

$$\begin{aligned} H =& \sum_{j=1}^{4} \omega_j \sigma_{jj} + \Omega a^\dagger a + \omega_m b^\dagger b - G a^\dagger a (b + b^\dagger) \\ &+ \lambda_1 (a^k \sigma_{12} + a^{\dagger k} \sigma_{21}) + \lambda_2 (a^k \sigma_{13} + a^{\dagger k} \sigma_{31}) \\ &+ \lambda_3 (a^k \sigma_{24} + a^{\dagger k} \sigma_{42}) + \lambda_4 (a^k \sigma_{34} + a^{\dagger k} \sigma_{43}), \end{aligned} \tag{1}$$

where $\sigma_{ij} = |i\rangle\langle j|$, a ($a^\dagger$) annihilates (creates) a cavity photon, and b ($b^\dagger$) acts on the mechanical mode. The optomechanical coefficient G controls the radiation-pressure coupling.

The sideband-resonance conditions used in the coarse-grained diamond model are

$$k\Omega = (\omega_1 - \omega_j) + \omega_m = (\omega_j - \omega_4) + \omega_m, \qquad j = 2, 3, \tag{2}$$

which imply $\omega_2 = \omega_3$. It is convenient to define

$$N_k = a^{\dagger k} a^k, \qquad M_k = a^k a^{\dagger k}. \tag{3}$$

The coarse-grained coherent Hamiltonian is written as

$$H_{\text{eff}} = H_{\text{Kerr}} + H_{\text{trip}} + H_{23} + H_{\text{Stark}}, \tag{4}$$

with

$$H_{\text{Kerr}} = -\frac{G^2}{\omega_m} (a^\dagger a)^2, \tag{5}$$

$$\begin{aligned} H_{\text{trip}} =& \frac{kG}{\omega_m} \Big[\lambda_1 (\sigma_{12} a^k b^\dagger + \sigma_{21} a^{\dagger k} b) + \lambda_2 (\sigma_{13} a^k b^\dagger + \sigma_{31} a^{\dagger k} b) \\ &+ \lambda_3 (\sigma_{24} a^k b^\dagger + \sigma_{42} a^{\dagger k} b) + \lambda_4 (\sigma_{34} a^k b^\dagger + \sigma_{43} a^{\dagger k} b) \Big], \end{aligned} \tag{6}$$

$$H_{23} = \frac{\lambda_1 \lambda_2}{\omega_m} (\sigma_{23} + \sigma_{32}) N_k - \frac{\lambda_3 \lambda_4}{\omega_m} (\sigma_{23} + \sigma_{32}) M_k, \tag{7}$$

and

$$\begin{aligned} H_{\text{Stark}} =& \frac{\lambda_1^2}{\omega_m} (\sigma_{22} N_k - \sigma_{11} M_k) + \frac{\lambda_2^2}{\omega_m} (\sigma_{33} N_k - \sigma_{11} M_k) \\ &+ \frac{\lambda_3^2}{\omega_m} (\sigma_{44} N_k - \sigma_{22} M_k) + \frac{\lambda_4^2}{\omega_m} (\sigma_{44} N_k - \sigma_{33} M_k). \end{aligned} \tag{8}$$

Equation (7) is the term that requires particular care. When $k = 1$, $M_1 = N_1 + 1$. Consequently, for equal couplings $\lambda_j = \lambda$, the intermediate-state term does not vanish; it

becomes $-(\lambda^2/\omega_m)(\sigma_{23}+\sigma_{32})$. Physically, the extra unity in $aa^\dagger$ reflects the bosonic commutator. Removing it by algebraic simplification would remove a real contribution to the level mixing.

The structure of the system is summarized in Fig. 1. The diagram is deliberately schematic: it shows the diamond transitions, the induced intermediate-state channel, and the coupling of the atom–field sector to the mechanical mode. The formal Hamiltonian contains k-photon operators, whereas the results reported later are restricted to $k = 1$.

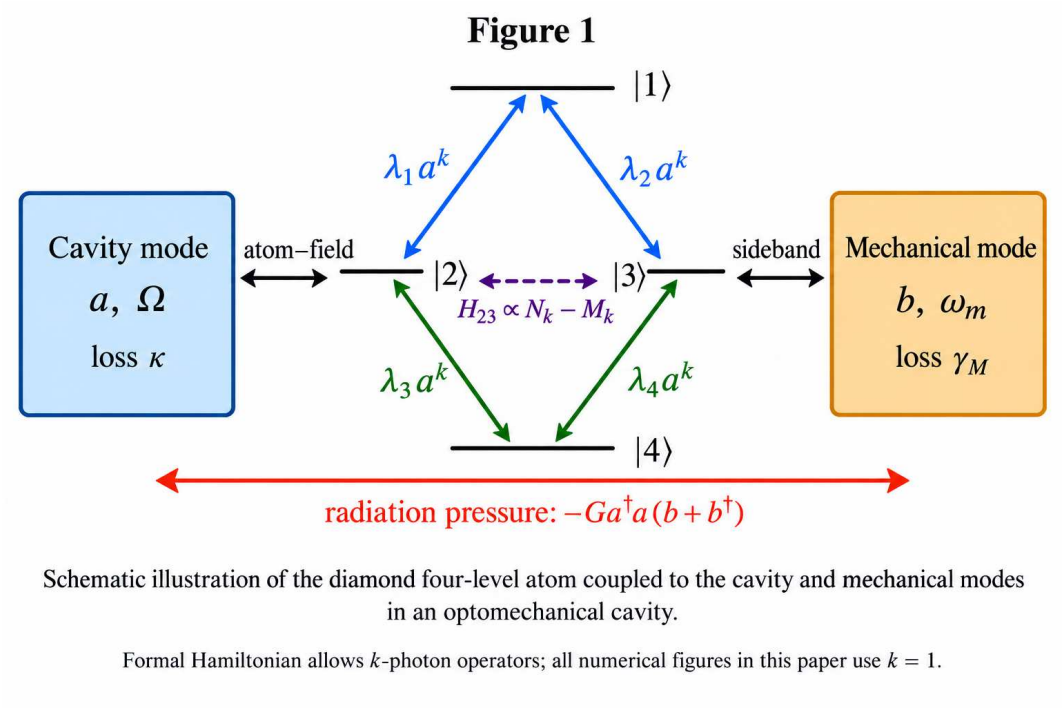


Figure 1: Schematic of the diamond four-level atom coupled to a cavity mode and a mechanical mode. The formal atom–field transitions contain k-photon operators, while the numerical results in this work use $k = 1$. The dashed $|2\rangle \leftrightarrow |3\rangle$ channel represents the induced coupling in Eq. (7).

To include losses at the level of conditioned trajectories, we use

$$H_{\rm nh} = H_{\rm eff} - \frac{i}{2}\Big[\kappa a^\dagger a + \gamma_M b^\dagger b + (\Gamma_1+\Gamma_2)\sigma_{11} + \Gamma_4\sigma_{22} + \Gamma_3\sigma_{33}\Big]. \tag{9}$$

This non-Hermitian Hamiltonian describes evolution conditioned on no detected jump. After each propagation step the state is normalized before reduced quantities are calculated. The resulting observables must therefore be interpreted as conditional no-jump quantities, not as unconditional ensemble averages.

3 Initial state and reduced atomic diagnostics

The phase to be estimated is encoded before the interaction begins,

$$|\psi_A(\phi)\rangle = \frac{|1\rangle + e^{i\phi}|2\rangle}{\sqrt{2}}. \tag{10}$$

The field and mechanical subsystems are initialized in Fock states $|n_0\rangle_F$ and $|m_0\rangle_M$, giving

$$|\Psi(0;\phi)\rangle = |\psi_A(\phi)\rangle \otimes |n_0\rangle_F \otimes |m_0\rangle_M. \tag{11}$$

After propagation with Eq. (9) and normalization, the reduced atomic density operator is

$$\rho_A(t;\phi) = \mathrm{Tr}_{F,M}\, |\Psi(t;\phi)\rangle\langle\Psi(t;\phi)|. \tag{12}$$

If $|\Psi\rangle = \sum_{\mu,\alpha} C_{\mu\alpha}|\mu\rangle_E|\alpha\rangle_A$, then

$$[\rho_A]_{\alpha\beta} = \sum_{\mu} C_{\mu\alpha} C^*_{\mu\beta}. \tag{13}$$

The phase derivative is evaluated numerically with a central difference,

$$\partial_\phi \rho_A \simeq \frac{\rho_A(\phi+\delta\phi) - \rho_A(\phi-\delta\phi)}{2\delta\phi}. \tag{14}$$

For $\rho_A = \sum_r p_r |r\rangle\langle r|$, the reduced-atomic QFI is

$$F_Q = 2\sum_{r,s} \frac{|\langle r|\partial_\phi \rho_A|s\rangle|^2}{p_r + p_s}, \qquad p_r + p_s > 0. \tag{15}$$

This quantity measures how well the encoded phase can be estimated using the atom alone after it has interacted with the other two subsystems.

We also calculate the atomic von Neumann entropy

$$S_A = -\,\mathrm{Tr}(\rho_A \log_2 \rho_A), \tag{16}$$

the purity

$$P = \mathrm{Tr}(\rho_A^2), \tag{17}$$

and the total l_1 coherence

$$C_{l_1} = \sum_{\alpha\neq\beta} |\rho_{\alpha\beta}|. \tag{18}$$

Entropy and purity are related measures of reduced-state mixedness, so their agreement is best viewed as a consistency check rather than as two independent entanglement witnesses. By contrast, C_{l_1} addresses the distribution of coherence among all pairs of atomic levels.

4 Numerical implementation and validation

The stationary calculation uses

$$\lambda_1 = \lambda_2 = \lambda_3 = \lambda_4 = 0.10, \qquad k = 1, \qquad \omega_m = 0.30, \tag{19}$$

$$\kappa = 0.01, \qquad \gamma_M = 0.01, \tag{20}$$

$$\Gamma_1 = 0.05, \quad \Gamma_2 = 0.03, \quad \Gamma_3 = 0.03, \quad \Gamma_4 = 0.01, \tag{21}$$

with initial Fock states $|n_0\rangle_F = |6\rangle_F$ and $|m_0\rangle_M = |8\rangle_M$. The coupling is scanned over $G = 0.1, 0.2, \ldots, 0.9$, and time is written as $\tau = \omega_m t$ over $0 \leq \tau \leq 30$.

The cavity and mechanical bases are truncated at $N_f = N_m = 14$. For $k = 1$, the tripartite exchange terms change (n, m) as $(n \mp 1, m \pm 1)$, so $n + m$ is conserved by the coherent exchange sector. Starting from $(n_0, m_0) = (6, 8)$, the connected manifold satisfies $n + m = 14$ and is fully contained in the chosen truncation. The time-independent Hamiltonian is propagated with a sparse Krylov matrix-exponential method. We take $\delta\phi = 10^{-4}$; representative calculations repeated with 10^{-3}, 5×10^{-4}, 10^{-4}, and 5×10^{-5} change the reported QFI only beyond the displayed precision.

Several simple benchmarks were imposed before interpreting the curves. At $\tau = 0$ the calculation returns $F_Q = 1$, $S_A = 0$, $P = 1$, $|\rho_{12}| = 1/2$, and $C_{l_1} = 1$, exactly as required by the initial pure atomic superposition. The coherent part of the assembled Hamiltonian is Hermitian to numerical precision. These checks do not prove that the effective model is valid in every parameter regime, but they do verify the internal numerical implementation used for the present scan.

A separate physical caveat concerns the largest values of G. At $G = 0.9$, the ratio G/ω_m reaches 3. Because Eqs. (1)–(7) are used in a coarse-grained effective description, the high-G end of the scan should be read as a sensitivity study unless the regime of validity of the coarse-graining approximation is established independently. We therefore avoid presenting the largest ratios as an experimentally validated strong-coupling limit.

5 Numerical results and physical discussion

Rather than placing many nearly overlapping curves in a single panel, we divide the time-domain results into two complementary coupling groups. The first group, $G = 0.1, 0.3, 0.5$, follows the evolution from weak to intermediate optomechanical coupling. The second group, $G = 0.5, 0.7, 0.9$, uses $G = 0.5$ as a common reference and then follows the system toward the high-coupling end of the formal scan. This paired presentation makes it easier to see which features disappear gradually, which persist, and which become almost insensitive to further increases of G. The separate coupling-summary figures use all nine values $G = 0.1, 0.2, \ldots, 0.9$ and therefore show the global trend without relying only on a few selected curves.

5.1 Local phase sensitivity

Figures 2 and 3 show the reduced-atomic QFI for the two coupling groups. At $G = 0.1$, the curve contains deep collapses and strong revivals. Physically, this means that phase information initially written into the atomic superposition is repeatedly transferred away from the atom and partially returned by the coherent interaction. The recovery is not complete at every revival, but the recurrent structure shows that the loss of local phase sensitivity is not simply monotonic.

Moving through $G = 0.3$ and 0.5, the revivals become less pronounced and the envelope

becomes smoother. The second comparison, $G = 0.5, 0.7, 0.9$, shows that this smoothing continues at larger coupling. Importantly, a smoother curve is not automatically a better metrological curve. The time-averaged QFI decreases continuously over the complete scan: $\overline{F}_Q = 0.450$ at $G = 0.1$, 0.433 at $G = 0.2$, 0.394 at $G = 0.3$, 0.367 at $G = 0.4$, 0.353 at $G = 0.5$, and then approaches a slowly varying high-G value, reaching 0.336 at $G = 0.9$. Figure 10 makes this monotonic reduction explicit. Thus, in the present parameter slice, stronger optomechanical coupling regularizes the temporal pattern but reduces the average phase information that can be extracted from the atom alone.

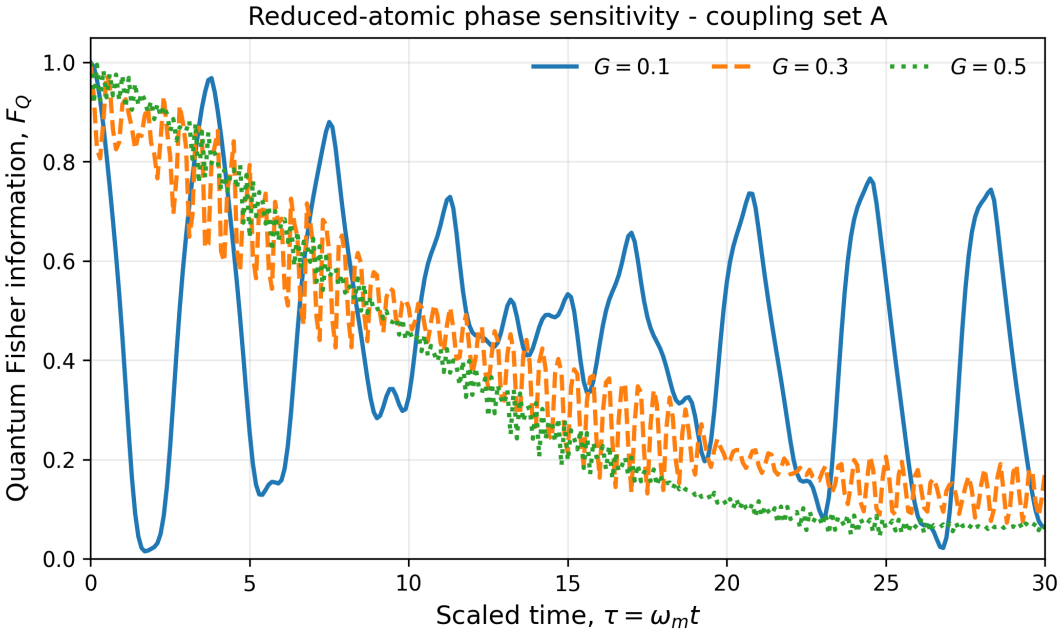


Figure 2: Reduced-atomic quantum Fisher information for $G = 0.1$, 0.3, and 0.5. This set emphasizes the change from the strongly oscillatory weak-coupling regime to the smoother intermediate-coupling dynamics.

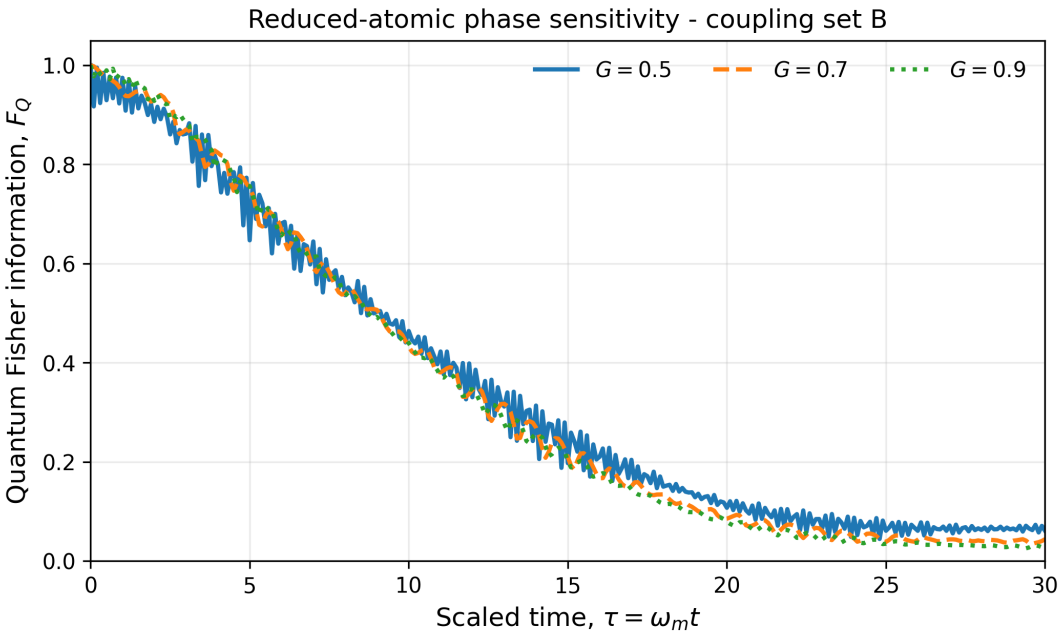


Figure 3: Reduced-atomic quantum Fisher information for $G = 0.5$, 0.7, and 0.9. The common $G = 0.5$ curve links the two QFI comparisons and shows how the high-G traces approach a smoother, lower-sensitivity regime.

5.2 Conditioned atom–rest entanglement

The entropy comparisons in Figs. 4 and 5 display a much stronger coupling dependence than the QFI. At $G = 0.1$, the reduced atomic entropy rises to about 1.676 bits, which is close to the maximum value of 2 bits available to a four-level subsystem. Along a normalized no-jump trajectory the total conditional state is pure, so this entropy directly measures entanglement between the atom and the combined field–mechanical subsystem.

As G increases, the highest entropy reached during the evolution falls rapidly. The full scan gives maxima of approximately 1.676, 1.436, 1.100, 0.954, 0.776, 0.648, 0.538, 0.447, and 0.374 bits from $G = 0.1$ to 0.9. The decrease is therefore not an artifact of choosing only the weakest and strongest curves. Figure 11 shows that it is a systematic trend over the entire scan. In physical terms, stronger G keeps the conditional atomic amplitudes less strongly correlated with mutually distinguishable field–mechanical components. This conclusion is specific to the post-selected no-jump branch and should not be read as a statement about unconditional Lindblad dynamics.

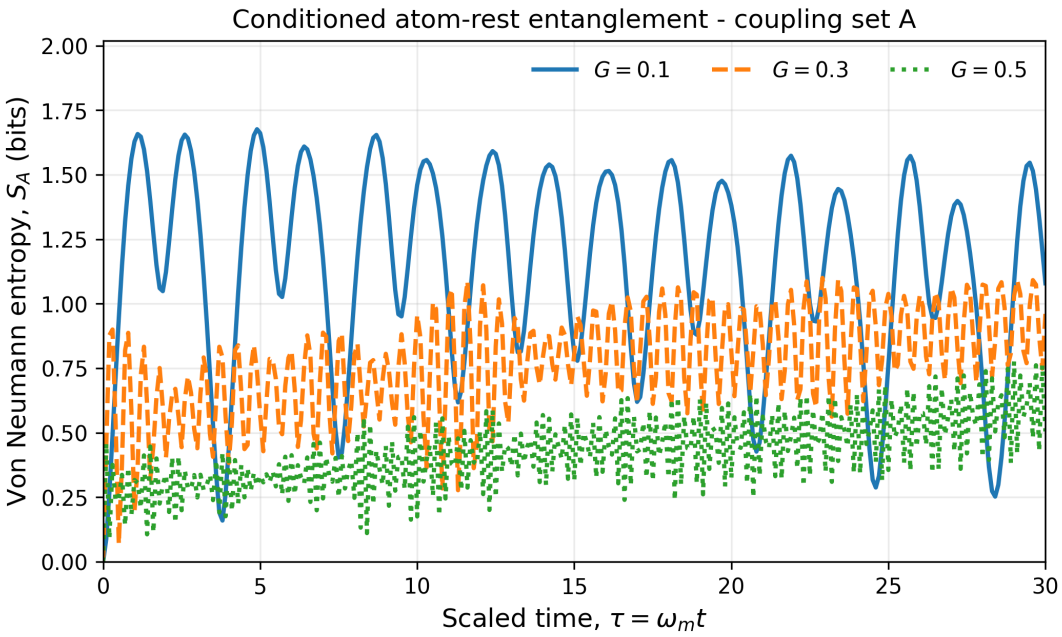


Figure 4: Reduced atomic von Neumann entropy for $G = 0.1$, 0.3, and 0.5. The progressive reduction of the entropy maxima shows the rapid suppression of conditioned atom–rest entanglement as the coupling moves away from the weak-G regime.

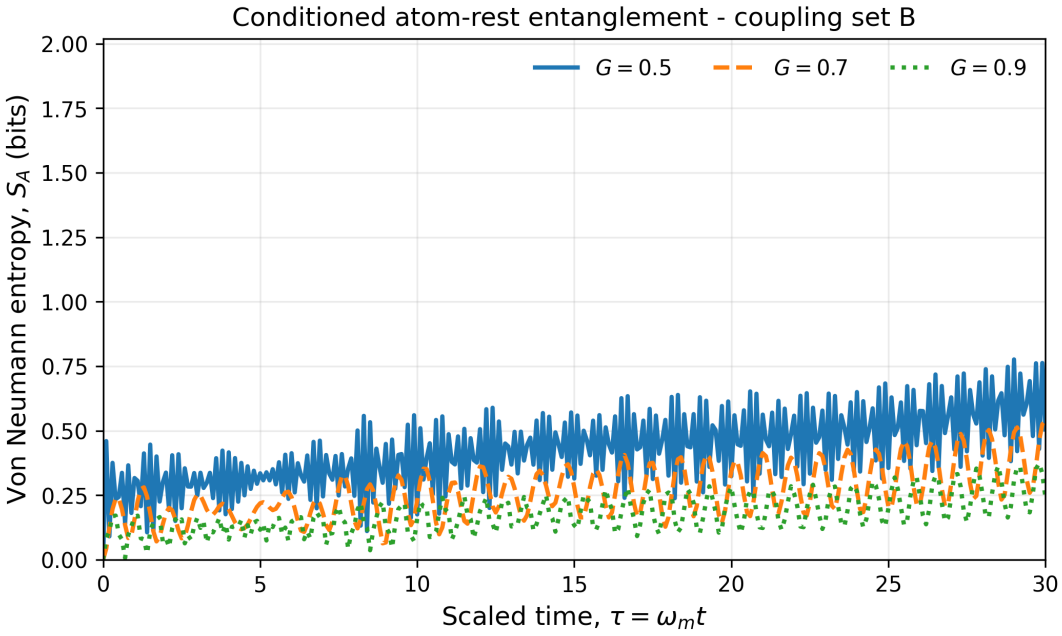


Figure 5: Reduced atomic von Neumann entropy for $G = 0.5$, 0.7, and 0.9. In the higher-coupling group the atomic subsystem remains substantially less entangled with the combined field–mechanical degrees of freedom.

5.3 Purity of the reduced atom

The purity curves in Figs. 6 and 7 provide the complementary view of the same reduced-state spectrum. The minimum purity rises from about 0.356 at $G = 0.1$ to 0.506 at $G = 0.3$ and 0.688 at $G = 0.5$. In the second group it continues upward, reaching 0.805 at $G = 0.7$ and 0.876 at

$G = 0.9$. The complete monotonic trend is shown in Fig. 12.

The entropy and purity results should be interpreted together rather than counted as independent demonstrations of two unrelated effects. Both tell us that the reduced atom is less mixed at larger G. What is more interesting is the comparison with QFI: the atomic state becomes purer while its average sensitivity to the encoded phase decreases. This illustrates a basic point of quantum estimation theory. Purity tells us how mixed a state is; QFI tells us how rapidly that state moves in state space when the parameter changes. A very pure state can still carry little information about a particular parameter if its dependence on that parameter is weak.

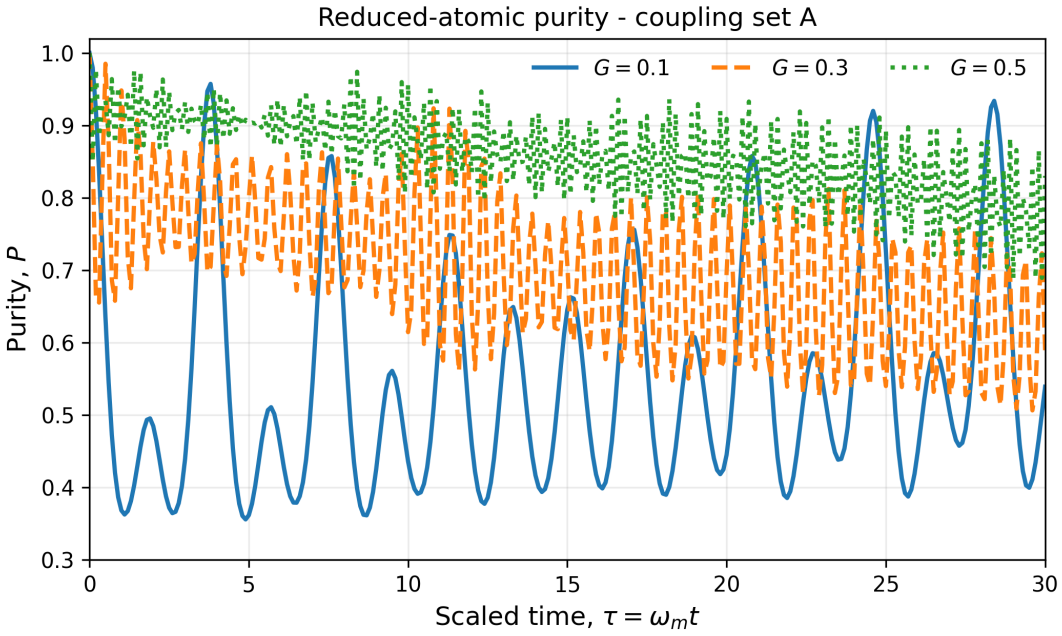


Figure 6: Reduced atomic purity for $G = 0.1$, 0.3, and 0.5. Increasing G raises the lower envelope of the purity and progressively limits the mixing of the conditioned atomic subsystem.

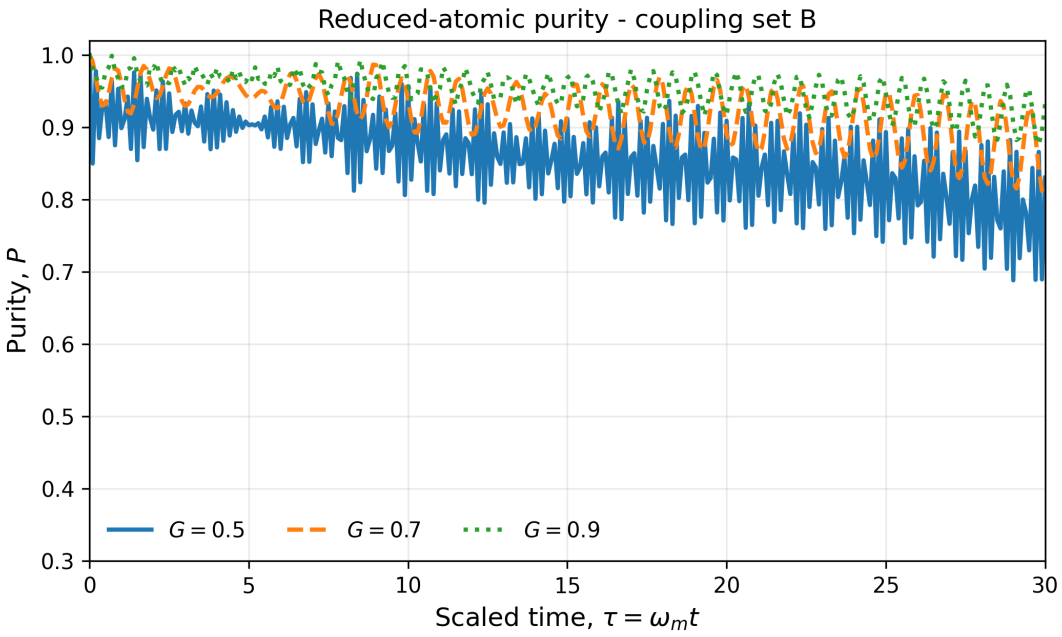


Figure 7: Reduced atomic purity for $G = 0.5$, 0.7, and 0.9. The high-G curves remain close to unity for much of the evolution, consistent with the reduced entropy seen in Fig. 5.

5.4 Redistribution of atomic coherence

The total l_1 coherence behaves differently from both the entanglement entropy and the purity. Figures 8 and 9 show that sizeable off-diagonal atomic coherence survives throughout the scan, but its detailed time dependence is rearranged as G changes. The time-averaged coherence first increases from about 1.162 at $G = 0.1$ to a maximum near 1.235 at $G = 0.3$, and then decreases gently toward 1.177 at $G = 0.9$. Figure 13 therefore confirms a weak, non-monotonic dependence on G rather than the strong monotonic behavior seen for entropy and purity.

This difference is physically reasonable for a four-level atom. The l_1 norm sums the magnitudes of all off-diagonal elements, so coherence can migrate between different pairs of levels. A reduction of $|\rho_{12}|$, for example, can be partly compensated by interaction-generated coherences involving $|3\rangle$ or $|4\rangle$. QFI is more selective because it measures sensitivity to the particular phase ϕ encoded in the initial $|1\rangle$–$|2\rangle$ superposition. The persistence of total coherence therefore does not contradict the decrease of local phase QFI; the remaining coherence is not necessarily aligned with the parameter direction relevant to the estimation task.

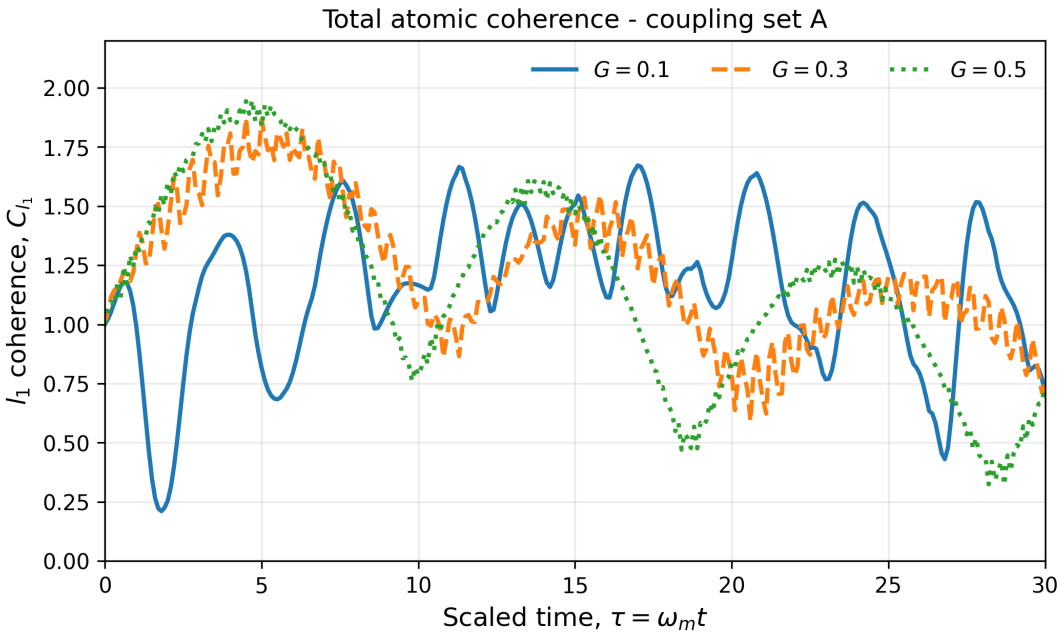


Figure 8: Total atomic l_1 coherence for $G = 0.1$, 0.3, and 0.5. The comparison shows that coherence is redistributed rather than uniformly suppressed as the optomechanical coupling increases.

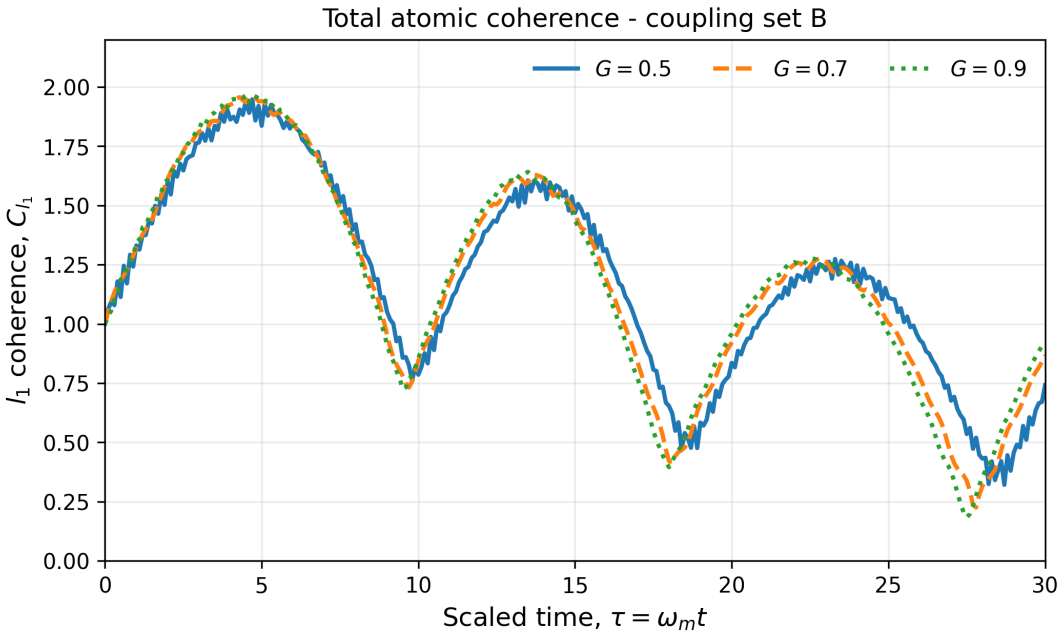


Figure 9: Total atomic l_1 coherence for $G = 0.5$, 0.7, and 0.9. The high-coupling traces remain of comparable overall magnitude even though the reduced-atomic QFI has already fallen appreciably.

5.5 Full coupling scan

Table 1 and Figs. 10–13 summarize all nine calculated values of G. These plots are important because they separate genuine coupling trends from features that may appear prominent in only one time trace. The mean QFI, maximum entropy, and minimum purity all change systematically with G: the first two decrease while the purity increases. The mean total coherence is the

exception, showing a shallow maximum around $G = 0.3$ and then a weak decline. Taken together, the four summaries show that the optomechanical coupling does not act as a universal "quantum-resource amplifier" or "resource suppressor." Instead, it redistributes different kinds of information and correlation in different ways.

Table 1: Aggregate diagnostics from the corrected stationary calculation. $\overline{F}_Q$ and $\overline{C}_{l_1}$ denote time averages over $0 \leq \tau \leq 30$. All nine sampled values of G are included.

G	$\overline{F}_Q$	$\max S_A$ (bits)	$\min P$	$\overline{C}_{l_1}$
0.1	0.450	1.676	0.356	1.162
0.2	0.433	1.436	0.425	1.222
0.3	0.394	1.100	0.506	1.235
0.4	0.367	0.954	0.587	1.203
0.5	0.353	0.776	0.688	1.187
0.6	0.345	0.648	0.753	1.181
0.7	0.340	0.538	0.805	1.179
0.8	0.337	0.447	0.846	1.177
0.9	0.336	0.374	0.876	1.177

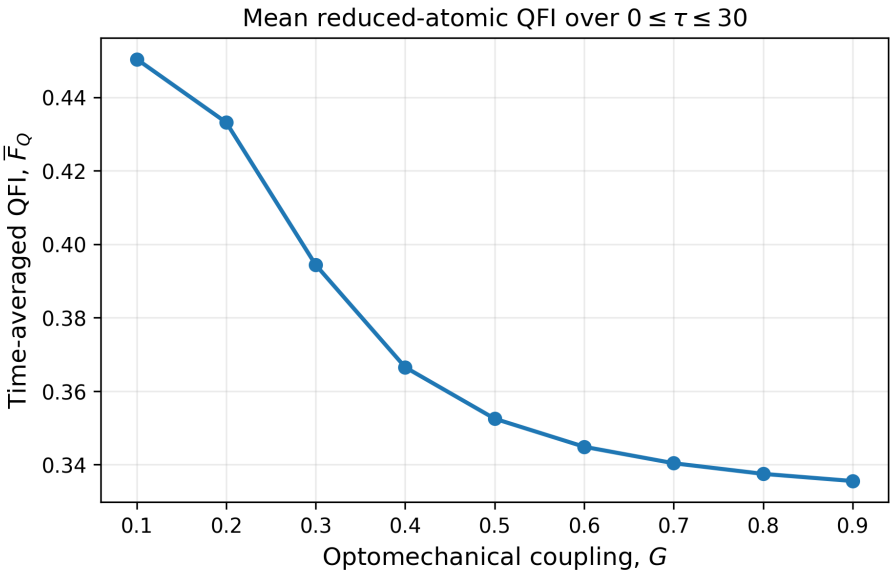


Figure 10: Time-averaged reduced-atomic QFI as a function of G using the full nine-point scan. The decrease is strongest at low-to-intermediate coupling and becomes more gradual at the high-G end.

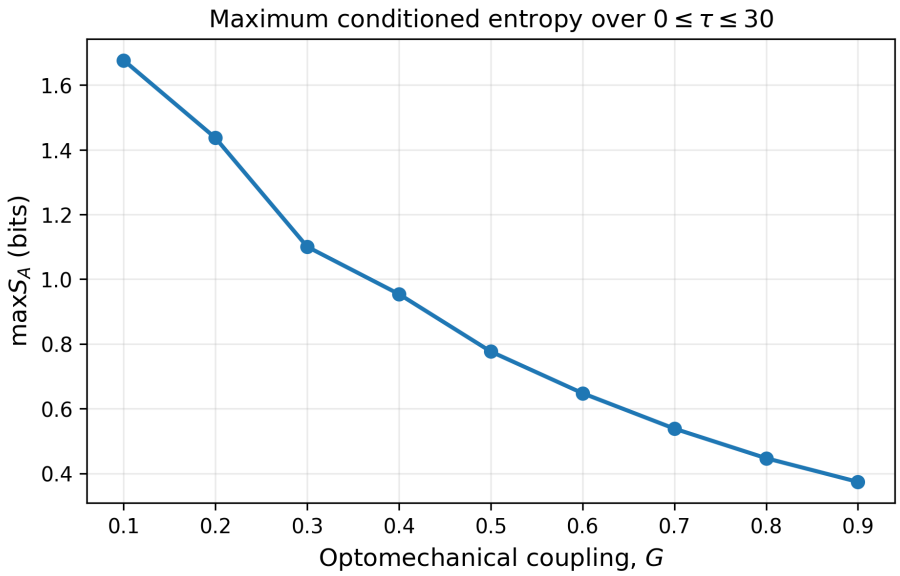


Figure 11: Maximum conditioned atom–rest entropy as a function of G. The monotonic decrease demonstrates that the entanglement suppression observed in the time traces persists throughout the complete coupling scan.

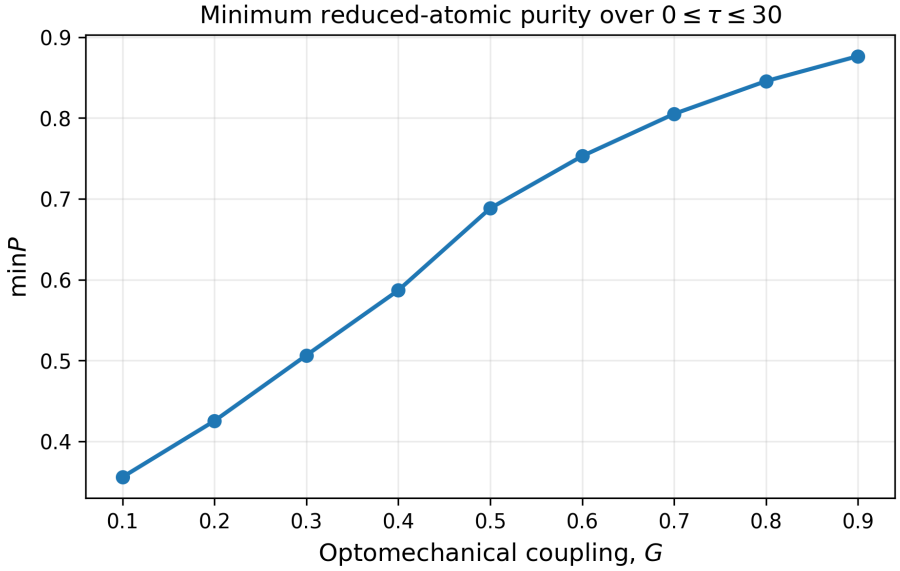


Figure 12: Minimum reduced-atomic purity as a function of G. The monotonic rise mirrors the entropy reduction and provides a direct measure of how the conditional atomic state remains less mixed at larger coupling.

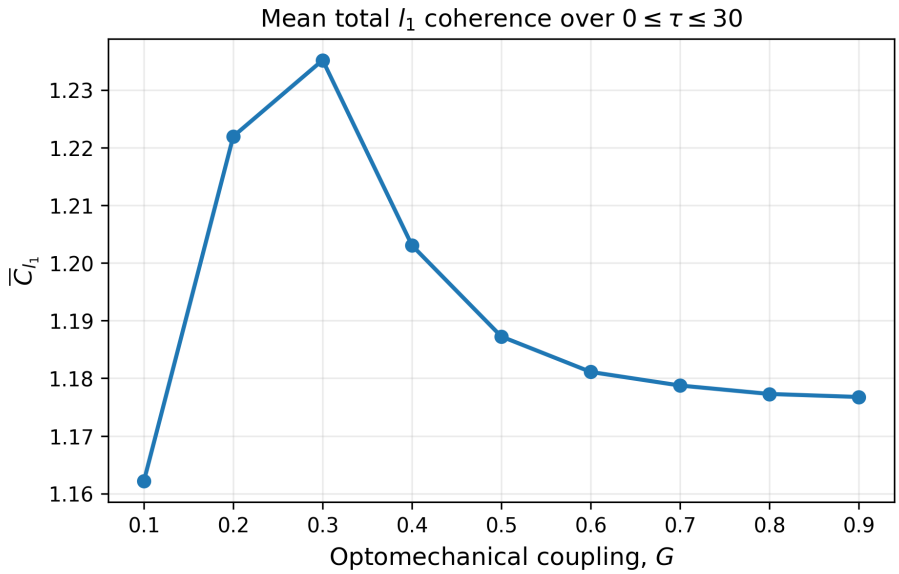


Figure 13: Time-averaged total atomic l_1 coherence as a function of G. Unlike QFI, entropy, and purity, the coherence is weakly non-monotonic and reaches a shallow maximum near $G = 0.3$.

6 Limitations and extensions

The present calculation is intentionally narrower than the formal Hamiltonian. First, the atom is stationary. A moving-atom extension should specify the cavity-mode profile, for example

$$g(t) = \sin\left(\frac{p\pi[z_0 + vt]}{L}\right), \tag{22}$$

with the initial position z_0, velocity v, mode index p, and dimensionless motional parameter defined independently. Comparing a stationary atom fixed at an antinode with a moving atom starting from a node changes more than one physical condition at once and does not isolate motion cleanly.

Second, although the Hamiltonian retains the formal k-photon operators, all figures in the present paper use $k = 1$. For $k > 1$, both the explicit factor k in the tripartite term and the factorial dependence contained in N_k and M_k can change the accessible manifolds and the time scales. A genuine multiphoton claim therefore requires separate, converged calculations for $k = 2$ and higher together with a careful scan of the initial photon number.

Third, Eq. (9) describes a normalized no-jump branch. A statement about unconditional open-system behavior would require a Lindblad master equation with the relevant jump operators. If the mechanical reservoir is at finite temperature, both thermal excitation and damping should be included. These extensions are physically worthwhile, but they are different calculations and should not be inferred from the conditional trajectories shown here.

Finally, the largest G/ω_m ratios deserve a controlled derivation or a restricted experimental comparison. The broad scan is useful because it reveals the qualitative sensitivity of the observables to G, but quantitative experimental claims should remain within a parameter range for which the effective coarse-grained Hamiltonian is justified.

7 Conclusion and outlook

We have examined a diamond four-level atom in an optomechanical cavity with the aim of separating three closely related but non-equivalent questions: how much of an initially encoded atomic phase remains locally measurable, how strongly the atom becomes entangled with the rest of the system, and how much atomic coherence survives after the interaction. Treating these questions together is important because a change that is favorable for one quantity need not be favorable for another.

A first technical conclusion concerns the structure of the effective Hamiltonian. The induced $|2\rangle \leftrightarrow |3\rangle$ coupling contains $N_k = a^{\dagger k}a^k$ and $M_k = a^k a^{\dagger k}$, and the two operators must remain distinct. For $k = 1$, their difference is the bosonic commutator itself. Retaining this operator ordering prevents the intermediate-state coupling from being accidentally removed when equal atom–field couplings are used. This correction is not merely algebraic bookkeeping; it changes the pathway through which amplitude and coherence move between the two intermediate levels and is therefore essential before QFI or entanglement curves are interpreted.

The numerical results then reveal a clear but nontrivial role for the optomechanical coupling. At weak G, the reduced atomic QFI undergoes strong collapse-and-revival behavior, showing that phase information can leave the atom and later return. As G grows, these revivals become smoother and the time-averaged local QFI decreases from about 0.450 to 0.336. The smoother curves at larger coupling should therefore not be described as a metrological enhancement. They represent a more regular time dependence, but the atom, on average, carries less information about the initially encoded phase.

The entropy and purity tell a different part of the story. Over the same coupling range, the maximum conditioned atom–rest entropy falls from about 1.676 to 0.374 bits, while the minimum atomic purity rises from about 0.356 to 0.876. Thus the atomic subsystem remains substantially less mixed at large G and becomes less entangled with the combined field–mechanical subsystem along the normalized no-jump trajectory. The important physical lesson is that reduced mixedness does not guarantee improved phase estimation. A state may be quite pure and still be only weakly sensitive to the parameter one wants to estimate. QFI depends on the direction in which the state changes with ϕ, not only on the length or purity of the state vector in an abstract sense.

The total l_1 coherence adds a further distinction. Its time-averaged value remains within a relatively narrow interval and changes non-monotonically with G. This indicates that the interaction mainly redistributes coherence among different level pairs rather than removing it uniformly. In a four-level atom, following a single off-diagonal matrix element can therefore be misleading. The atom may retain a substantial amount of coherence even when the particular phase information encoded in the initial $|1\rangle$–$|2\rangle$ superposition becomes less accessible locally. This is why coherence and QFI, although related, need not follow the same trend.

The combined message of the expanded figure set is consequently more specific than a general claim of "enhancement" or "suppression." Stronger optomechanical coupling, for the stationary single-photon parameter set studied here, suppresses conditioned atom–rest entanglement and keeps the atom purer, but it does not preserve local phase sensitivity and it does not monotonically

control total atomic coherence. The optomechanical interaction therefore acts as a redistribution mechanism: it changes where information and correlations reside within the hybrid system rather than moving all quantum resources in the same direction.

From a practical point of view, the expanded G comparisons also identify where the dynamics change most rapidly. The strongest reduction of entanglement and the largest loss of mean local QFI occur before the scan reaches its highest values; above roughly $G = 0.6$, the QFI changes only slowly while purity continues to improve. This separation suggests that an intermediate coupling window may be more informative than simply pushing G to the largest available value. If the goal is local phase estimation, weaker coupling retains more QFI; if the goal is to keep the conditional atom relatively pure and weakly entangled with the remaining modes, larger coupling is favorable. The appropriate operating point therefore depends on the quantum task rather than on a single notion of stronger coupling.

Several extensions follow naturally from this result. A moving atom should be studied with a fully specified spatial mode function so that motion is varied without changing the initial coupling condition. Genuine multiphoton dynamics require independent converged scans for $k > 1$ rather than an extrapolation from the $k = 1$ case. Finally, unconditional dissipative behavior should be addressed with a Lindblad master equation, especially when finite-temperature mechanical noise is relevant. These additions would allow the present conditional stationary calculation to serve as a controlled baseline for a broader study of phase metrology and correlation flow in multilevel optomechanical systems.

Data availability

No data are available for this study.

Code availability

No code is available for this study.

Funding

The authors received no specific grant or external funding for this work.

Author contributions

S. Jamal Anwar conceived and developed the study, organized the physical model and numerical analysis, interpreted the results, and prepared the original manuscript. S. Abdul Khalek contributed to the analytical interpretation, critical review of the model and results, and revision of the manuscript. Both authors reviewed and approved the final manuscript and accept responsibility for the content of the work.

Conflict of interest / competing interests

The authors declare that they have no known competing financial interests or personal relationships that could have appeared to influence the work reported in this paper.

Ethics approval

Not applicable. This work is a theoretical and numerical study and did not involve human participants, human data, animals, or biological samples.

Consent to participate

Not applicable.

Consent for publication

Both authors have read and approved the final manuscript and consent to its publication.

Acknowledgments

None.

References

[1] E. T. Jaynes and F. W. Cummings, "Comparison of quantum and semiclassical radiation theories with application to the beam maser," *Proceedings of the IEEE* **51**, 89–109 (1963).

[2] B. W. Shore and P. L. Knight, "The Jaynes–Cummings model," *Journal of Modern Optics* **40**, 1195–1238 (1993).

[3] P. Meystre and M. Sargent, *Elements of Quantum Optics* (Springer, Berlin, 2007).

[4] J. H. Eberly, N. B. Narozhny, and J. J. Sanchez-Mondragon, "Periodic spontaneous collapse and revival in the quantum Jaynes–Cummings model," *Physical Review Letters* **44**, 1323–1326 (1980).

[5] N. B. Narozhny, J. J. Sanchez-Mondragon, and J. H. Eberly, "Coherence versus incoherence: Collapse and revival in a simple quantum model," *Physical Review A* **23**, 236–247 (1981).

[6] G. Rempe, H. Walther, and N. Klein, "Observation of quantum collapse and revival in a one-atom maser," *Physical Review Letters* **58**, 353–356 (1987).

[7] P. L. Knight and P. M. Radmore, "Quantum revivals of a two-level system driven by chaotic radiation," *Physics Letters A* **90**, 342–346 (1982).

[8] S. J. D. Phoenix and P. L. Knight, "Fluctuations and entropy in models of quantum optical resonance," *Annals of Physics* **186**, 381–407 (1988).

[9] V. Buzek and I. Jex, "Dynamics of a two-level atom in a Kerr-like medium," *Optics Communications* **78**, 425–435 (1990).

[10] S. Haroche and J. M. Raimond, *Exploring the Quantum: Atoms, Cavities, and Photons* (Oxford University Press, Oxford, 2006).

[11] R. Miller, T. E. Northup, K. M. Birnbaum, A. Boca, A. D. Boozer, and H. J. Kimble, "Trapped atoms in cavity QED: coupling quantized light and matter," *Journal of Physics B* **38**, S551–S565 (2005).

[12] A. Joshi and S. V. Lawande, "Effect of the Kerr-like medium on the dynamics of a two-photon Jaynes–Cummings model," *Physical Review A* **42**, 1752–1756 (1990).

[13] M. S. Abdalla, M. M. A. Ahmed, and A. S. F. Obada, "Influence of a Kerr-like medium on the evolution of a three-level atom in a two-mode squeezed vacuum state," *Physica A* **170**, 393–410 (1991).

[14] G. S. Agarwal, *Quantum Optics* (Cambridge University Press, Cambridge, 2013).

[15] C. C. Gerry and P. L. Knight, *Introductory Quantum Optics* (Cambridge University Press, Cambridge, 2005).

[16] M. O. Scully and M. S. Zubairy, *Quantum Optics* (Cambridge University Press, Cambridge, 1997).

[17] E. Paspalakis and P. L. Knight, "Phase control of spontaneous emission," *Physical Review Letters* **81**, 293–296 (1998).

[18] A. B. Bhattacherjee, "Cavity quantum electrodynamics of a trapped atom in a degenerate four-level diamond configuration," *Journal of Physics B* **40**, 3669–3680 (2007).

[19] H. R. Baghshahi, M. K. Tavassoly, and A. Behjat, "Entropy squeezing and atomic inversion in the k-photon Jaynes–Cummings model in the presence of the Stark shift and a Kerr medium," *Chinese Physics B* **23**, 074203 (2014).

[20] S. E. Harris, "Electromagnetically induced transparency," *Physics Today* **50**, 36–42 (1997).

[21] M. Fleischhauer, A. Imamoglu, and J. P. Marangos, "Electromagnetically induced transparency: Optics in coherent media," *Reviews of Modern Physics* **77**, 633–673 (2005).

[22] A. Imamoglu, H. Schmidt, G. Woods, and M. Deutsch, "Strongly interacting photons in a nonlinear cavity," *Physical Review Letters* **79**, 1467–1470 (1997).

[23] H. J. Kimble, "The quantum internet," *Nature* **453**, 1023–1030 (2008).

[24] A. Einstein, B. Podolsky, and N. Rosen, "Can quantum-mechanical description of physical reality be considered complete?," *Physical Review* **47**, 777–780 (1935).

[25] J. S. Bell, "On the Einstein Podolsky Rosen paradox," *Physics* **1**, 195–200 (1964).

[26] C. H. Bennett, D. P. DiVincenzo, J. A. Smolin, and W. K. Wootters, "Mixed-state entanglement and quantum error correction," *Physical Review A* **54**, 3824–3851 (1996).

[27] W. K. Wootters, "Entanglement of formation of an arbitrary state of two qubits," *Physical Review Letters* **80**, 2245–2248 (1998).

[28] S. J. D. Phoenix and P. L. Knight, "Establishment of an entangled atom-field state in the Jaynes–Cummings model," *Physical Review A* **44**, 6023–6029 (1991).

[29] A. Ekert and P. L. Knight, "Entangled quantum systems and the Schmidt decomposition," *American Journal of Physics* **63**, 415–423 (1995).

[30] W. H. Zurek, "Decoherence, einselection, and the quantum origins of the classical," *Reviews of Modern Physics* **75**, 715–775 (2003).

[31] H. P. Breuer and F. Petruccione, *The Theory of Open Quantum Systems* (Oxford University Press, Oxford, 2002).

[32] L. Amico, R. Fazio, A. Osterloh, and V. Vedral, "Entanglement in many-body systems," *Reviews of Modern Physics* **80**, 517–576 (2008).

[33] R. Horodecki, P. Horodecki, M. Horodecki, and K. Horodecki, "Quantum entanglement," *Reviews of Modern Physics* **81**, 865–942 (2009).

[34] T. J. Kippenberg and K. J. Vahala, "Cavity optomechanics: Back-action at the mesoscale," *Science* **321**, 1172–1176 (2008).

[35] M. Aspelmeyer, T. J. Kippenberg, and F. Marquardt, "Cavity optomechanics," *Reviews of Modern Physics* **86**, 1391–1452 (2014).

[36] F. Marquardt and S. M. Girvin, "Optomechanics," *Physics* **2**, 40 (2009).

[37] J. D. Teufel *et al.*, "Sideband cooling of micromechanical motion to the quantum ground state," *Nature* **475**, 359–363 (2011).

[38] K. Hammerer, A. S. Sorensen, and E. S. Polzik, "Quantum interface between light and atomic ensembles," *Reviews of Modern Physics* **82**, 1041–1093 (2010).

[39] D. Hunger *et al.*, "Resonant coupling of a Bose–Einstein condensate to a micromechanical oscillator," *Physical Review Letters* **104**, 143002 (2010).

[40] A. Nimmrichter, K. Hornberger, and K. Hammerer, "Optomechanical sensing of spontaneous wave-function collapse," *Physical Review Letters* **113**, 020405 (2014).

[41] M. Ludwig, A. H. Safavi-Naeini, O. Painter, and F. Marquardt, "Enhanced quantum nonlinearities in a two-mode optomechanical system," *Physical Review Letters* **109**, 063601 (2012).

[42] P. Treutlein, D. Hunger, S. Camerer, T. W. Hansch, and J. Reichel, "Bose–Einstein condensate coupled to a nanomechanical resonator on an atom chip," *Physical Review Letters* **99**, 140403 (2007).

[43] C. Genes, D. Vitali, and P. Tombesi, "Emergence of atom-light-mirror entanglement inside an optical cavity," *Physical Review A* **77**, 050307 (2008).

[44] C. W. Helstrom, *Quantum Detection and Estimation Theory* (Academic Press, New York, 1976).

[45] A. S. Holevo, *Probabilistic and Statistical Aspects of Quantum Theory* (North-Holland, Amsterdam, 1982).

[46] V. Giovannetti, S. Lloyd, and L. Maccone, "Quantum-enhanced measurements: Beating the standard quantum limit," *Science* **306**, 1330–1336 (2004).

[47] V. Giovannetti, S. Lloyd, and L. Maccone, "Advances in quantum metrology," *Nature Photonics* **5**, 222–229 (2011).

[48] P. Hyllus *et al.*, "Fisher information and multipartite entanglement," *Physical Review A* **85**, 022321 (2012).

[49] G. Toth, "Multipartite entanglement and high-precision metrology," *Physical Review A* **85**, 022322 (2012).

[50] V. Vedral, M. B. Plenio, M. A. Rippin, and P. L. Knight, "Quantifying entanglement," *Physical Review Letters* **78**, 2275–2279 (1997).

[51] M. A. Nielsen and I. L. Chuang, *Quantum Computation and Quantum Information* (Cambridge University Press, Cambridge, 2000).

[52] L. Pezze and A. Smerzi, "Entanglement, nonlinear dynamics, and the Heisenberg limit," *Physical Review Letters* **102**, 100401 (2009).

[53] J. Ma, X. Wang, C. P. Sun, and F. Nori, "Quantum spin squeezing," *Physics Reports* **509**, 89–165 (2011).

[54] F. Daneshmand, H. R. Baghshahi, and S. Y. Mirafzali, "Quantum Fisher information and entanglement of a dissipative hybrid optomechanical system with multi-photon transition," *Quantum Information Processing* **23**, 226 (2024).

[55] F. Daneshmand, H. R. Baghshahi, and S. Y. Mirafzali, "Quantum Fisher information of a diamond-type four-level atom interacting with a single-mode quantized field in an optomechanical cavity," *Communications in Theoretical Physics* **77**, 045105 (2025).

[56] S. L. Braunstein and C. M. Caves, "Statistical distance and the geometry of quantum states," *Physical Review Letters* **72**, 3439–3443 (1994).

[57] M. G. A. Paris, "Quantum estimation for quantum technology," *International Journal of Quantum Information* **7**, 125–137 (2009).

[58] G. Toth and I. Apellaniz, "Quantum metrology from a quantum information science perspective," *Journal of Physics A* **47**, 424006 (2014).

[59] T. Baumgratz, M. Cramer, and M. B. Plenio, "Quantifying coherence," *Physical Review Letters* **113**, 140401 (2014).

[60] A. Streltsov, G. Adesso, and M. B. Plenio, "Colloquium: Quantum coherence as a resource," *Reviews of Modern Physics* **89**, 041003 (2017).

[61] J. Dalibard, Y. Castin, and K. Molmer, "Wave-function approach to dissipative processes in quantum optics," *Physical Review Letters* **68**, 580–583 (1992).

[62] K. Molmer, Y. Castin, and J. Dalibard, "Monte Carlo wave-function method in quantum optics," *Journal of the Optical Society of America B* **10**, 524–538 (1993).

[63] H. J. Carmichael, *An Open Systems Approach to Quantum Optics* (Springer, Berlin, 1993).

[64] D. F. Walls and G. J. Milburn, *Quantum Optics*, 2nd ed. (Springer, Berlin, 2008).

[65] C. K. Law, "Interaction between a moving mirror and radiation pressure: A Hamiltonian formulation," *Physical Review A* **51**, 2537–2541 (1995).

[66] S. Bose, K. Jacobs, and P. L. Knight, "Preparation of nonclassical states in cavities with a moving mirror," *Physical Review A* **56**, 4175–4186 (1997).

[67] W. Marshall, C. Simon, R. Penrose, and D. Bouwmeester, "Towards quantum superpositions of a mirror," *Physical Review Letters* **91**, 130401 (2003).

[68] D. Vitali *et al.*, "Optomechanical entanglement between a movable mirror and a cavity field," *Physical Review Letters* **98**, 030405 (2007).

[69] I. Wilson-Rae, N. Nooshi, W. Zwerger, and T. J. Kippenberg, "Theory of ground state cooling of a mechanical oscillator using dynamical backaction," *Physical Review Letters* **99**, 093901 (2007).

[70] F. Marquardt, J. P. Chen, A. A. Clerk, and S. M. Girvin, "Quantum theory of cavity-assisted sideband cooling of mechanical motion," *Physical Review Letters* **99**, 093902 (2007).